Current Source Density Estimation Enhances the Performance of Motor-Imagery related Brain-Computer Interface

Dheeraj Rathee*, Haider Raza, Girijesh Prasad *Senior Member, IEEE*, Hubert Cecotti *Senior Member, IEEE*

***Abstract*—The objective is to evaluate the impact of EEG referencing schemes and spherical surface Laplacian (SSL) methods on the classification performance of motor-imagery (MI) related brain-computer interface systems. Two EEG referencing schemes: common referencing, common average referencing (CAR) and three surface Laplacian methods: current source density (CSD), finite difference method, and SSL using realistic head model, were implemented separately for pre-processing of the EEG signals recorded at the scalp. A combination of filter bank common spatial filter for features extraction and support vector machine for classification was used for both pairwise binary classifications and four-class classification of MI tasks. The study provides three major outcomes: (i) the CSD method performs better than CR providing a significant improvement of 3.02 % and 5.59 % across six binary classification tasks and four-class classification task, respectively; (ii) the combination of a greater number of channels at the pre-processing stage as compared to the feature extraction stage yields better classification accuracies for all the Laplacian methods; (iii) the efficiency of all the surface Laplacian methods reduced significantly in the case of a fewer number of channels considered during the pre-processing.**

***Index Terms*—Motor imagery, Brain-computer interface, Pre-processing, Spatial filtering, Spherical surface Laplacian.**

I. Introduction

Electroencephalographic oscillations, recorded over the scalp, can be the basis of alternative modes of communication and control, in particular as brain-computer interfaces (BCIs) [1], [2], [3]. Non-invasive EEG-based BCI systems acquire neural signals at scalp level, analyse them to evaluate specific features of EEG activity that are related to voluntary imagery/execution tasks and, finally utilise the outcomes as control signals that are further relayed to efferent devices. During the past few decades, these systems hold a significant amount of research interest due to the relative ease of conducting experiments, inexpensiveness, and minimal risk to participants. In general, there are two ways to generate the class-specific features. Firstly, time-domain potentials generated in response to specialized external stimulation (e.g., P300, steady-state evoked potentials, and evoked potentials), implemented in case of reactive BCI systems [4], [5]. Secondly, features generated from spontaneous brain signals generated during the performance of endogenous tasks, for instance, motor imagery (MI), emotion imagery, and mental arithmetic tasks, considered during active BCI paradigms [6], [7]. The latter approach of BCI implementation is highly popular, in particular, MI-related BCI which is one of the most explored EEG-based paradigms [8], [9], [10].

The overall performance of MI-related BCI system depends on various factors, e.g., pre-processing of the raw brain signals, extraction of information (features) related to the motor task, and finally the application of the extracted features to the output device (controlling process). Most of the current research studies focus on feature extraction algorithms and their optimization for performance improvement although pre-processing operations can affect the performance of the system significantly [11], [12], [13]. The pre-processing stage generally involves cleaning the raw EEG data for unwanted artefacts (e.g., external noise, muscular, and ocular interferences) and/or reducing the effect of volume conduction (VC) and non-stationarity from scalp acquired EEG signals [14], [15]. All these measures account for the significant increase in the signal-to-noise ratio (SNR) and hence improvise the performance of BCI systems. The complex multi-dimensional EEG data recorded at scalp level provide a direct inference of the electrical activity associated within a large neuronal population of the brain cortex. VC results from the mixing of spatial-temporal information generated at the cortical sources of the brain as the tissues and bone structure between the brain cortex and the scalp induce superimposition of electrophysiological dynamics of the signal [16], [17].

Several measures can be applied for minimizing the effect of volume conduction at scalp level recordings. Different referencing schemes (e.g., Common referencing (CR), Bipolar, Common average referencing (CAR)) and Laplacian filtering methods (e.g., Hjorth, spline surface Laplacian methods) have been implemented earlier for this purpose [18], [19], [20], [21], [22] (for further details refer to [23]). Apart from these, independent component analysis (ICA) [24], principal component analysis (PCA) [25], and advanced source localization techniques (i.e. beamforming, sLORETA) [26], [27] have been utilised for enhancement of the BCI performance. Additionally, recent studies using source localization techniques have shown that linear inverse transforms can be applied in real time and have shown significant improvement in motor imagery task classification [28], [29], [30]. The Laplacian filtering can contribute to the enhancement of SNR by reducing the spatial noise [31] and hence assists in constraining the potential

Manuscript received August 12, 2016; revised April 6, 2017. Corresponding author: D. Rathee (email: rathee-d@email.ulster.ac.uk).

D. Rathee, G.Prasad, and H. Cecotti are with the Intelligent Systems Research Centre, School of Computing & Intelligent Systems, Ulster University, Derry∼Londonderry, N. Ireland, UK.

H. Raza is with the Farr Institute of Health Informatics Research, Swansea University Medical School, Swansea, UK.

sources of brain activity [32]. The surface Laplacian has spatial bandpass characteristics that depend on factors such as the spacing of the electrodes and any spatial smoothing of the particular implementation of the Laplacian being considered. Signals such as sensorimotor rhythms are often focused (i.e., they have a relatively high spatial frequency) relative to artifacts such as eye blinks and EKG. In addition, since the surface Laplacian emphasizes local sources, it minimizes the signal components volume conducted from distant sources. The surface Laplacian also improves spatial resolution [33] and thus can aid source identification. The role of the surface Laplacian in source constraint can be evaluated in part by the extent to which it produces signals that are uncorrelated.

Prior research studies that involve qualitative comparison of different spatial transformation methods often restrict their analysis to different algorithms or to different parameters for the same algorithm (e.g., different parameters of CSD, source imaging techniques, or different ICA algorithms) [31], [32], [34]. Other published works emphasize on the theoretical perspectives during comparing different referencing schemes or Laplacian filtering methods, with little or no consideration of their impact on BCI performance [35], [36]. Although the findings of these studies may contribute significantly in the optimisation of the algorithms, limited information has been provided for the BCI researchers regarding improvement in classification accuracies. A recent study showed enhancement of binary classification accuracies during motor imagery task with CAR implementation as compared to CR [37]. However, the findings of the study are preliminary (only 5 subjects and two classes) and did not include spline based Laplacian methods, which recently attracted a lot of EEG-based studies [20], [38].

In this paper, we evaluate the impact of two referencing schemes: CR (left mastoid) and CAR, and three spherical surface Laplacian (SSL) filtering methods: current source density (CSD) [20], [39], finite difference method (SS_F) [38], and SSL using realistic head model (SS_R) [22], on the classification performance of MI-based BCI systems. The raw EEG signal was pre-processed separately using above mentioned five methods and SVM classifier has been implemented for binary and multi-class classifications based on features generated by filter-bank CSP algorithm. Furthermore, the effect of reducing the number of the channels at the pre-processing level and at feature extraction level has also been studied. Here, we have not considered the discrete methods such as the Hjorth's Laplacian [19], which is a planar scheme (i.e., subtracting the linearly-weighted potential of the nearest neighbors) as the estimates fail at the edges of a two-dimensional montage, effectively reducing the number of channels with available EEG data [31], [40]. Thus, implementation of Hjorth's Laplacian may restrict the analysis as the availability of the pre-processed EEG channels will not be uniform across the different competing methods. Additionally, a study involving empirical comparison of various spatial filtering methods showed better performance of CAR as compared to small laplacian method [41].

The remainder of this paper is organized as follows: Section II provides a detailed description of the various referencing schemes and Laplacian methods applied for pre-processing the raw EEG data. Section III describes the EEG dataset included in the study and applied methodology with complete signal processing pipeline. Section IV illustrates the results of Spatial and temporal analysis, comparison of performances of FBCSP based MI-BCI, and effect of the different combinations of number of channels selected during pre-processing and feature extraction step. Section V provides a discussion of the outcomes, impact, and limitation of this study along with possible future enhancements.

II. Referencing and Laplacian filtering Methods

A. Common Reference(CR)

Scalp EEG signal acquisition systems use differential amplifiers by taking the measurements of two electrodes (the main channel and a reference channel) as input and generate a signal for the corresponding EEG channel as the difference between the two inputs with subsequent amplification. The choice of input electrodes to each amplifier is known as a montage. The most basic montage is CR, where the potential difference at each electrode in the montage is computed with a common reference, for instance, left mastoid, right mastoid or ear lobe.

B. Common Average Reference(CAR)

The CAR scheme can be implemented by subtracting the average potential of all EEG channels from scalp potential of each channel. The method enhances the SNR by reducing the noise common to all the channels [42]. If the scalp potentials are assumed to be generated by point sources, and the whole head is uniformly covered by EEG channels (symmetrically and equally spaced), the CAR transforms the scalp potential distribution into a zero-mean spatial potential distribution [42]. Although the assumptions of uniform and complete channel coverage as well as point sources are generally difficult to manage in practice, the referencing scheme still provides nearly reference free scalp EEG recordings. The CAR montage can be implemented according to the equation,

$$b_i \quad = \quad a_i - \sum_{j=1}^{N} (a_j/N) \tag{1}$$

where $a_i \in \mathbb{R}^{1\times T}$ is the potential difference between i^th channel and a common reference, N is the number of channels, and T is the number of time samples in each channel data.

C. Current Source Density (CSD) Method

Current source densities (CSDs) over the scalp can be estimated by the method presented by Perrin et al. [20], [39], with spherical spline interpolations. The process involves the projection of the real scalp surface onto the sphere followed by spherical interpolation of the scalp potentials using spherical spline surfaces. Let us consider the similar case as of Section II-B. The cosine distance between different pairs of electrode interpolation locations can be calculated by:

$$\cos(P,Q) = 1 - \frac{(x_P - x_Q)^2 + (y_P - y_Q)^2 + (z_P - z_Q)^2}{2} \tag{2}$$

where the Cartesian coordinates of the channel locations P and Q are (x_P, y_P, z_P) and (x_Q, y_Q, z_Q), respectively. Further, the transformation matrices can be obtained using the following expressions:

$$H(l) = -\frac{1}{4\pi}\sum_{n=1}^{\infty}\left(\frac{(2n+1)^2}{n^m(n+1)^m}\right)\cdot K_n(l) \quad (3)$$

$$G(l) = \frac{1}{4\pi}\sum_{n=1}^{\infty}\left(\frac{2n+1}{n^m(n+1)^m}\right)\cdot K_n(l) \quad (4)$$

where, $K_n(l)$ is the Legendre polynomial of degree n, and m is the spline flexibility index. In this study, we choose the values of n and m as 50 and 4, respectively. It should be noted that the values of $K_n(l)$ can be calculated by the following recurrence relation:

$$(n+1)K_{n+1}(l) = (2n+1)K_n(l) - nK_{n-1}(l) \quad (5)$$

The transformation matrices have to be estimated only once, based on the Cartesian coordinates of the electrode locations. Finally, the current source densities can be determined by implementing the equation as below

$$C(E) = \sum_{i=1}^{N} c_i H(cos(E, E_i)) \quad (6)$$

where, E is the particular spherical projection and c_i a computable constant for the i^{th} electrode, can be obtained by solving following equations:

$$\begin{aligned}(G+\lambda)C + Tc_0 &= A \\ T'C &= 0\end{aligned} \quad (7)$$

where,

$$\begin{aligned}T' &= [1, 1, \ldots, 1] \\ C' &= [c_1, c_2, ..., c_N] \\ A' &= [a_1, a_2, ..., a_N] \\ G &= (G_{i,j}) = G(\cos(E_i, E_j)) \\ \lambda &= \text{smoothing constant}(1.0e-5)\end{aligned}$$

The estimation process of CSDs involves three major steps. The first step is to generate two transformation matrices termed G and H using Eqs. (3), (4), and (5). These transformation matrices depend only on the number and relative position of surface locations included in the EEG montage (i.e., their cosine distances), which can be estimated using Eq. (2). For this reason, these matrices have to be computed only once for any given EEG montage. The second step is to compute the constant vector (c_i) using Eq. (7). The length of the constant vector is equal to number of electrodes in the EEG montage. The final step is to compute the CSD values for each EEG channel data using Eq. (6).

D. Finite-difference (SS_F) method

The SS_F method, presented by Oostendorp et al. [38], provides the approximation of surface Laplacian operator on a triangulated $3D$ spherical surface. Thus, an interpolation for scalar functions on a rectangular grid on a planar surface is extended to the interpolation function on a closed three-dimensional triangulated surface. If the potential is measured in a regular rectangular grid, the surface Laplacian $L_s(i,j)$ at grid point (i,j) can be estimated by averaging the acquired potentials $a(k,l)$ at the direct neighbors of (i,j) using:

$$L_s = \frac{1}{d^2}(a_{i-1,j} + a_{i+1,j} + a_{i,j-1} + a_{i,j+1} - 4a_{i,j}) \quad (8)$$

where, d is the distance between the nodes in the grid.

If the grid of known potential values is irregular, the above method can be replaced by one of the methods proposed by Huiskamp [43], in which the value of the surface Laplacian at electrode position lo can be estimated from appropriately weighted potential readings of the direct neighbors at positions l_i in a triangular grid, where $i \in \{1, \ldots, M\}$, and M is the number of direct neighbors. This approximation can be expressed by:

$$L_s = \frac{4}{\bar{r}\eta}\sum_{i=1}^{M}\left(\frac{1-\cos(\phi_i^-)}{\sin(\phi_i^-)} + \frac{1-\cos(\phi_i^+)}{\sin(\phi_i^+)}\right)\cdot \frac{1}{r_i}(a_i - a_0) \quad (9)$$

where, r_i is the length of vector $\vec{r_i} = \vec{l_i} - \vec{l_0}$, $\bar{r}$ is the mean value of r_i over all M direct neighbors of $\vec{l_0}$. ϕ_i^- is the angle from $\vec{r_{i-1}}$ to $\vec{r_i}$ and ϕ_i^+ is the angle from $\vec{r_i}$ to $\vec{r_{i+1}}$. η is a normalization factor and given as:

$$\eta = \sum_{i=1}^{M}\left(\frac{1-\cos(\phi_i^-)}{\sin(\phi_i^-)} + \frac{1-\cos(\phi_i^+)}{\sin(\phi_i^+)}\right) \quad (10)$$

E. Spline surface Laplacian filtering for Realistic head geometry(SS_R)

The SS_R method has the advantage of being readily applicable to the surfaces defined by MRI-based triangular meshes without the help of any intermediate representations, and it does not require any coordinate transformations as well [22]. The implementation of SS_R involves a two-step operation. The first step is to estimate a continuous potential distribution function $F(r)$ using the discrete inputs from various EEG electrode locations using a $3D$ polyharmonic spline interpolation scheme (Eq. 11), identical to the spherical spline Laplacian [17].

$$F(r) = \sum_{i=1}^{N} pK_{m-1}^i(r) + Q_{m-1} \quad (11)$$

where, $K_{m-1}^i(r)$ is a polyharmonic radial basis function, Q_{m-1} (osculating polynomial) acts as a smoothing function for the spline, and p is the spline coefficient.

In the second step, the SL operator ∇_s^2 is created over a defined underlying surface, using the Laplace-Beltrami operator ∇^2, which takes the form of the trace of the function's Hessian

$$L_s(F) = \nabla_s^2(F) = tr\left[\nabla\nabla F\right] \quad (12)$$

where, $tr[.]$ is the trace operator.

By explicitly removing the surface normal component from the gradient of the function $F(r)$, the operator is restricted to

This article has been accepted for publication in a future issue of this journal, but has not been fully edited. Content may change prior to final publication. Citation information: DOI 10.1109/TNSRE.2017.2726779, IEEE Transactions on Neural Systems and Rehabilitation Engineering

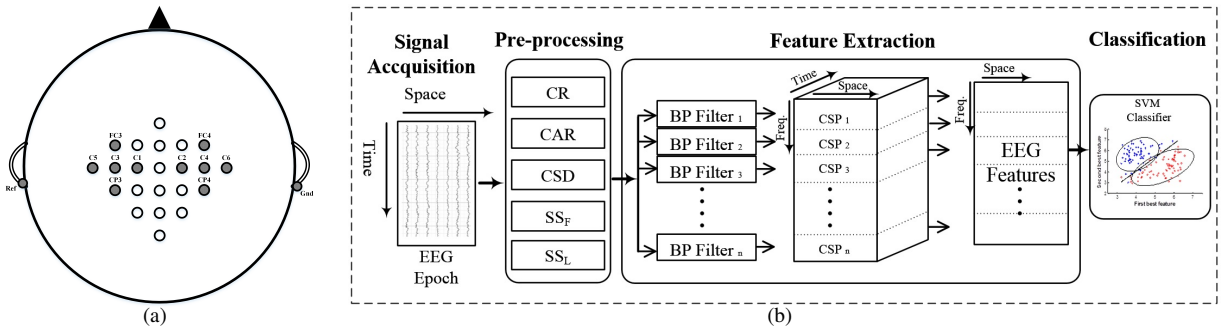

Fig. 1. (**a**) Montage of the acquired EEG data representing the 22 sensors used for pre-processing, and the 10 sensors used for feature extraction. (**b**) System overview with the different processing steps.

the surface tangent plane. Further, SL is considered to be the negative of the resulting operator to facilitate visualization and source analysis [17].

$$\nabla_s^2(F) = -tr\left[\nabla(I - n'n)\nabla F\right] \quad (13)$$

$$\nabla_s^2(F) = -tr\left[\nabla\nabla F\right] + tr\left[\nabla(n'n)\nabla F\right] \quad (14)$$

The second term on the right side of the above equation can be further expanded as,

$$tr\left[\nabla(n'n)\nabla F\right] = n(\nabla\nabla F)n' + n(tr[\nabla n]).\nabla F + (\nabla F)'(\nabla n)n' \quad (15)$$

The three expanded terms on the right side of Eq. 15 utilize distinct levels of geometrical variations: information of surface normals n, the trace of the curvature tensor ∇n, and the complete form of geometry (i.e., Jacobian matrix of surface normals). Furthermore, for generating analytical expression of the SS_R the surface is discretized using triangular mesh form, where vertices and edges represent the continuous surface geometry.

On a general surface given by a triangular mesh, the interpolation points are defined on the vertices of each triangle. The vertex normal can be generated from the surrounding triangle face normal while the weighting of a particular triangle face normal is set to be inversely related to the face area of that triangle [44]. To estimate the Jacobian matrix at each triangle vertex, the one-ring neighbors of a particular vertex is estimated at first, followed by calculation of the finite difference of vertex positions and unit normal vectors on these vertices.

III. Material and Methods

A. EEG Dataset

The BCI competition-IV [45], dataset 2A is a publically available MI related EEG dataset. The dataset comprised of 4 classes (left hand, right hand, both feet, and tongue) MI from nine subjects namely [A01-A09]. Two sessions, one for training and one for evaluation, were recorded from each subject. The data were recorded with 22 monopolar EEG channels (with left mastoid as reference and right mastoid as ground) and 3 monopolar electrooculogram (EOG) channels. In this study, we have selected 10 channels near motor cortex as depicted in Fig. 1(a), for feature extraction.

B. Filter Bank Common Spatial Pattern (FBCSP)

The filter bank common spatial pattern (FBCSP) is a widely used feature extraction algorithm. FBCSP is an extension of the common spatial pattern (CSP), where n different bandpass filters are used at the first stage to decompose the data into multiple frequency bands in the temporal domain [46]. CSP is typically used to create spatial filters for detecting Event-Related Desynchronization/Synchronization (ERD/ERS). A total of 10 bandpass filters in MI-related frequency range are used ([8-12], [10-14], [12-16],. . . ,[26-30]) for creating the filter bank.

C. Signal processing

According to Fig. 1 (b) in MI related EEG-based BCI, the following steps have been implemented for task detection: raw EEG signal acquisition, pre-processing, feature extraction (i.e. temporal and spatial filtering), and classification. Initially, raw EEG signals from the complete set of 22 channels have been considered and then pre-processing has been performed to improve the spatial resolution using each of the following methods: CR, CAR, CSD, SS_F, and SS_R. For SS_R, we used the default head MRI model provided with the SSLtool toolbox [47]. Further, in feature extraction stage, a bandpass filter bank has been applied to decompose the EEG signals into different frequency bands (FBs) by employing an 8^{th} order, zero-phase forward and reverse bandpass Butterworth filter. A total of 10 bandpass filters with overlapping bandwidths, including [8-12], [10-14], [12-16], [14-18], [16-20], [18-22], [20-24], [22-26], [24-28], [26-30] Hz, are used to process the data from 10 EEG channels. Later, spatial filtering has been performed on each FBs, which helps to maximize the divergence of bandpass filtered signals under one class, and minimize the divergence for the other class. In MI-related BCI systems, both physical and imaginary movements cause a growth of bounded neural rhythmic activity known as ERD/ERS. The CSP algorithm is widely used for calculating spatial patterns for detecting (ERD/ERS) [46]. Each combination of the bandpass filter and CSP algorithm calculates the discriminative features that are distinct to the particular frequency range. After doing CSP filtering, the discriminating features have been extracted using a time window of 3 seconds after the cue onsets. This particular time segment is responsible

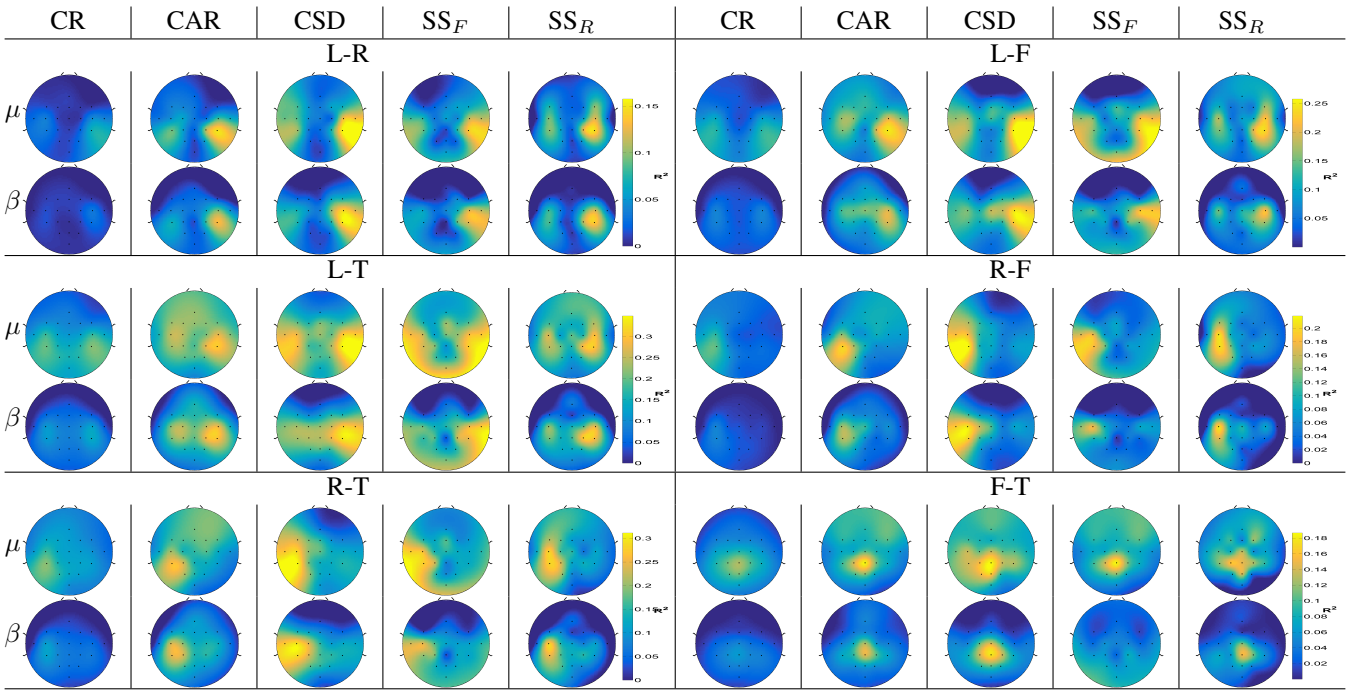

Fig. 2. Topographical plots representing the grand average correlation values (R^2) between average bandpower values (within μ-band (8-12Hz) and β-band (13-30Hz)) for six binary classification tasks and five referencing methods. R^2 values were averaged over subjects and sessions and scalp plotted for all 22 electrodes.

for bagging MI related ERD/ERS activities. The features obtained after applying CSP algorithms from all FBs are merged to create the set of input features for training/testing a classifier. Finally, the performance evaluation is obtained by measuring the accuracies for both two-class (i.e. the six pairwise binary classification tasks including four classes) and four-class BCI approaches using a linear SVM classifier. For the four-class approach, features were generated in one-versus-rest condition and four linear SVM classifiers were implemented for estimation of classification accuracies. In our study, we trained the classifiers on the features of the first session, while evaluated the performance on the second session. Moreover, we repeated the whole process for three different configurations of channel selection (i.e. 22/22, 22/10, and 10/10). We use the couple (N_{s0}/N_{s1}) to denote the number of sensors that are used for pre-processing (N_{s0}) and for feature extraction (N_{s1}).

The computational work has been performed on an Intel Core i7-4790 with 16 GB of memory, using in-house programs written in MATLAB V8.1 (The Mathworks, Natick, MA). The Matlab codes for implementing three SSL methods have been obtained from publicly available toolboxes(CSD toolbox [48], SSLtool [22], and Fieldtrip [47]).

IV. Results

A. Spatial and temporal analysis

To study the topographical responses of the methods, we implemented a similar approach published in a recent study [15]. bivariate Pearsons correlation coefficients (R) between class target (i.e., a dummy variable, coded -1 and $+1$) and band-power features in μ (8-12Hz) and β (13-30Hz) frequency bands for each electrode have been generated. These values were estimated for each binary task pair, subject, and session for 3 s of MI related period. Further group averaged R^2 values (across subjects and sessions) were estimated and scalp plotted over the 22 channel EEG montage for all pairwise binary classification tasks and referencing methods in μ and β frequency bands (see Fig. 2). The maplimit for all the topoplots within a pairwise binary task is kept same for making the plots comparable across various referencing methods and frequency bands. Fig. 2 clearly depicts higher values of correlation for CAR, CSD, SS$_F$ and SS$_R$ as compared to CR. Also, for most of the pairs of classes, CSD topographic plots showed relatively bigger yellow color spots as compared to other methods. This evidently suggests that CSD provided better spatial localization and higher values of R^2. Furthermore, time evolution plots of the averaged and normalized envelopes of EEG signals (for μ and β frequency bands) from C3 and C4 channel for the four imagery classes are presented in Fig. 3. Here, we included EEG data segment from 0 to 6 s from each trial, including both the rest state and motor imagery state. The envelope of the time series has been obtained using absolute values of Hilbert transformed signals. The envelope plots show better separability between two classes for three Laplacian and CAR methods as compared to CR.

B. BCI performances

The SVM-based accuracies (in %) for each pairwise binary classification task are presented in Tables I. Here, the CR method has been selected as a baseline method for pairwise comparisons with other methods. Wilcoxon signed rank test reveals a statistically significant ($p < 0.05$, FDR corrected for multiple comparisons) difference between the baseline method

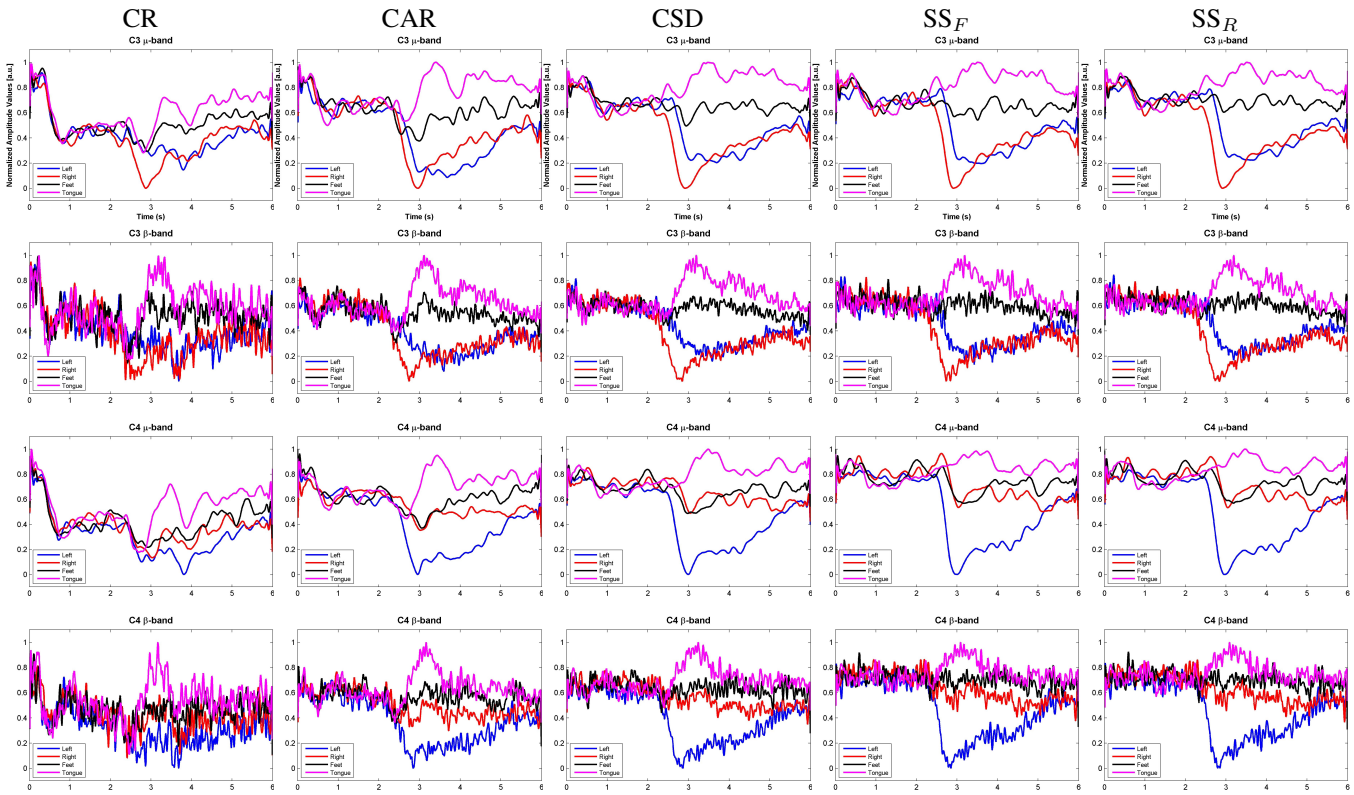

Fig. 3. Time-Evolution plots of the bandpassed EEG signal envelopes for the μ-band and β-band of the C3 and C4 channels for the four imagery tasks. The envelopes have been computed for both rest state and MI state (0 to 6 s). The values are normalized between 0 and 1. [a.u.: arbitrary units]

and CSD for all the binary classification tasks except for left vs. tongue whereas CAR, SS$_F$, and SS$_R$ failed to provide consistent results. Furthermore, the differences between the six binary classifications were evaluated to examine if there exists a combination of two MI tasks among the four that would emerge better than others but this evaluation showed no statistically significant difference across the six binary classification results. Table II provides the mean(SD) (across six binary tasks) of classification accuracies for the five referencing schemes. The results in Table II clearly showed CSD provided highest accuracies for eight out of nine subjects. The average performance across subjects and the six binary classification tasks is 78.75 ± 11.81, 79.33 ± 11.53, 82.36 ± 11.04, 77.48 ± 12.23, and 78.06 ± 11.93 for CR, CAR, CSD, SS$_F$ and SS$_R$ methods, respectively. By considering all the six binary tasks together, i.e., with 54 samples for each preprocessing method, pairwise comparisons indicate a significant difference between the baseline and the CSD method (p<10e-8).

The classification accuracies for four-class BCI approach are presented in Table III. The average performance across subjects is 52.55 ± 12.66, 53.51 ± 11.12, 58.14 ± 9.64, 52.74 ± 10.49, and 52.28 ± 9.59 for CR, CAR, CSD, SS$_F$ and SS$_R$ methods, respectively (chance level accuracy=25%). Here, the CR method has been selected as a baseline method for pairwise comparisons with other methods. Wilcoxon signed rank test reveals a statistically significant difference between the baseline method and CSD ($p = 0.0039$) whereas other comparisons failed to provide significant differences. Moreover, CSD enhances the four-class BCI accuracy by more than 5%.

C. Impact of altered number of channels at preprocessing stage and feature extraction stage

The performances of three channel-selection configurations ((22/10), (10/10), and (22/22)) at the pre-processing stage and feature extraction stage , have been evaluated for CAR, CSD, SS$_F$, and SS$_R$, and the results are depicted in Fig 4. The mean accuracies across the six binary classification tasks, for each configuration, are 79.33 ± 11.53, 76.20 ± 11.89, and 75.96 ± 12.40 for CAR; 82.36 ± 11.05, 79.69 ± 11.99, and 77.67 ± 13.54 for CSD; 77.48 ± 12.23, 75.46 ± 12.74, and 76.45 ± 13.07 for SS$_F$; 78.06 ± 11.93, 75.68 ± 13.02, and 77.27 ± 12.82 for SS$_R$. Pairwise comparisons with false discovery rate (FDR) correction indicated that the (22/10) system provides the best performance for both CAR and CSD while (22/22) results in worst performance. Although for SS$_F$, the pattern is different as we found no statistically significant difference between (22/10) and (22/22) whereas (10/10) configuration performed worst. Besides, SS$_F$'s performance is significantly better in (22/10) when compared with (10/10). For SS$_R$, however, we found no significant differences across the three configurations.

D. Impact of the position of CSD in the EEG signal processing pipeline

The impact of the performance related to the position of CSD was evaluated by comparing different feature extraction

This article has been accepted for publication in a future issue of this journal, but has not been fully edited. Content may change prior to final publication. Citation information: DOI 10.1109/TNSRE.2017.2726779, IEEE Transactions on Neural Systems and Rehabilitation Engineering

TABLE I
CLASSIFICATION ACCURACY (IN %) FOR THE CONFIGURATION (22/10): SIX PAIRWISE BINARY CLASSIFICATION RESULTS OBTAINED BY USING LINEAR SVM CLASSIFIER. STATISTICAL SIGNIFICANCE ($p - values$) HAS BEEN ESTIMATED USING WILCOXON SIGNED RANK TEST.

Subj.	Left vs. Right					Left vs. Feet					Left vs. Tongue				
	CR	**CAR**	**CSD**	**SS**$_F$	**SS**$_R$	**CR**	**CAR**	**CSD**	**SS**$_F$	**SS**$_R$	**CR**	**CAR**	**CSD**	**SS**$_F$	**SS**$_R$
A01	90.97	91.67	93.06	91.67	88.19	97.22	96.53	97.92	95.83	87.50	88.19	92.36	93.06	95.83	96.53
A02	61.11	61.81	68.06	59.03	56.94	75.00	74.31	81.94	69.44	75.00	72.22	68.75	72.22	65.28	65.28
A03	90.97	87.50	93.06	90.28	93.75	86.81	88.19	90.28	88.89	94.44	93.75	91.67	93.75	88.89	87.50
A04	69.44	70.83	77.08	77.08	67.36	75.00	83.33	87.50	79.17	75.00	86.11	88.89	87.50	88.89	89.58
A05	70.83	72.22	72.22	65.97	60.42	65.28	63.19	68.06	64.58	65.97	75.69	75.00	77.08	71.53	62.50
A06	65.28	62.50	65.97	64.58	64.58	70.83	68.75	70.83	70.83	65.97	66.67	66.67	70.83	65.28	65.97
A07	68.75	70.83	78.47	64.58	80.56	81.94	85.42	88.89	83.33	84.03	94.44	90.28	90.28	90.28	84.03
A08	92.36	95.14	97.22	95.83	95.83	75.00	79.17	77.08	77.08	87.50	83.33	79.86	84.03	68.06	76.39
A09	90.28	86.81	90.28	86.81	76.39	90.97	76.39	91.67	83.33	86.81	97.22	95.14	97.92	93.06	97.22
Mean	77.78	77.70	**81.71**	77.31	76.00	79.78	79.48	**83.80**	79.16	80.25	84.18	83.18	**85.19**	80.79	80.56
SD	12.99	12.68	11.87	14.12	14.53	10.26	10.21	10.05	9.93	10.17	10.66	10.85	9.81	12.88	13.53
***p*-value**	-	0.979	0.006	0.624	0.478	-	0.949	0.004	0.869	0.820	-	0.307	0.176	0.122	0.154
Subj.	Feet vs. Tongue					Right vs. Feet					Right vs. Tongue				
	CR	**CAR**	**CSD**	**SS**$_F$	**SS**$_R$	**CR**	**CAR**	**CSD**	**SS**$_F$	**SS**$_R$	**CR**	**CAR**	**CSD**	**SS**$_F$	**SS**$_R$
A01	75.69	73.61	76.39	76.39	70.14	93.75	96.53	95.14	95.14	94.44	97.92	97.92	97.92	97.22	98.61
A02	77.78	75.69	83.33	63.89	79.86	68.75	76.39	90.28	68.75	68.75	66.67	69.44	70.83	64.58	70.83
A03	65.97	78.47	70.14	77.08	79.86	86.11	89.58	86.81	80.56	70.83	97.22	95.14	97.22	89.58	88.19
A04	68.06	71.53	68.06	67.36	70.83	83.33	87.50	93.75	90.28	90.97	76.39	86.11	84.72	84.72	72.22
A05	59.03	59.72	66.67	55.56	61.11	64.58	65.28	66.67	72.22	62.50	69.44	73.61	72.22	64.58	70.83
A06	63.89	63.19	70.83	61.81	64.58	73.61	72.92	74.31	70.83	59.03	60.42	65.28	65.28	65.97	67.36
A07	77.78	76.39	79.86	78.47	76.39	95.14	97.22	97.92	96.53	96.53	89.58	97.22	94.44	90.97	97.92
A08	85.42	84.03	87.50	70.83	71.53	72.22	74.31	77.78	82.64	77.08	65.28	62.50	68.06	56.94	86.11
A09	86.81	74.31	92.36	77.78	83.33	62.50	64.58	65.97	61.11	77.08	93.75	92.36	96.53	86.81	77.08
Mean	73.38	72.99	**77.24**	69.91	73.07	77.78	80.48	**83.18**	79.78	77.47	79.63	82.18	**83.02**	77.93	81.02
SD	9.67	7.48	9.12	8.24	7.41	12.22	12.58	12.31	12.47	13.78	15.00	14.45	13.89	14.76	12.04
***p*-value**	-	0.333	0.004	0.071	0.720	-	0.003	0.001	0.273	0.793	-	0.131	0.008	0.278	0.765

TABLE II
AVERAGE CLASSIFICATION ACCURACIES (IN %) FOR FIVE REFERENCING SCHEMES ACROSS SIX BINARY TASKS. THE GRAND MEAN, SD AND $p - values$ ARE ESTIMATED BY CONSIDERING ALL THE SIX BINARY TASKS AND NINE SUBJECTS TOGETHER (I.E. 54 ACCURACY VALUES). STATISTICAL SIGNIFICANCE HAS BEEN ESTIMATED USING WILCOXON SIGNED RANK TEST.

Subj.	**CR**	**CAR**	**CSD**	**SS**$_F$	**SS**$_R$
A01	90.62	91.44	**92.25**	92.01	89.24
A02	70.25	71.06	**77.78**	65.16	69.44
A03	86.81	88.43	**88.54**	85.88	85.76
A04	76.39	81.37	**83.10**	81.25	77.66
A05	67.48	68.17	**70.49**	65.74	63.89
A06	66.78	66.55	**69.68**	66.55	64.58
A07	84.61	86.23	**88.31**	84.03	86.57
A08	78.94	79.17	81.94	75.23	**82.41**
A09	86.92	81.60	**89.12**	81.48	82.99
Grand Mean	78.76	79.33	**82.36**	77.48	78.06
SD	11.81	11.53	11.04	12.23	11.92
***p*-value**	-	0.2067	**1.29e-08**	0.1067	0.4779

TABLE III
CLASSIFICATION ACCURACY (IN %) FOR THE CONFIGURATION (22/10): 4-CLASS CLASSIFICATION RESULTS OBTAINED BY USING LINEAR SVM CLASSIFIERS IN ONE-VERSUS-REST CONFIGURATION. THE CHANCE LEVEL ACCURACY IS 25%. STATISTICAL SIGNIFICANCE ($p - values$) HAS BEEN ESTIMATED USING WILCOXON SIGNED RANK TEST.

Subj.	**CR**	**CAR**	**CSD**	**SS**$_F$	**SS**$_R$
A01	65.97	**68.05**	67.70	63.54	66.31
A02	36.46	43.06	**49.65**	44.79	42.71
A03	57.99	51.74	58.33	**59.03**	53.13
A04	50.35	57.99	**58.68**	44.79	56.60
A05	37.50	42.36	**48.26**	36.81	40.28
A06	37.85	42.71	**43.40**	42.01	40.97
A07	60.42	61.81	**66.32**	58.33	60.42
A08	56.94	44.44	58.68	**63.19**	48.96
A09	69.44	69.44	**72.22**	62.15	61.11
Mean	52.55	53.51	**58.14**	52.74	52.28
SD	12.66	11.12	9.64	10.49	9.59
***p*-value**	-	0.5313	**0.0039**	1	0.9141

systems: 1) FBCSP only, 2) CSD on the raw signal and then FBCSP, 3) bandpass filtering followed by CSD on each frequency band and then CSP, 4) same as 3 but without CSP, i.e. with bandpower features only, and 5) CSD on the raw EEG data followed by bandpower feature extraction. The variations of performance in relation to the place of CSD in the signal processing pipeline are depicted in Fig. 5, by considering the set of 22 channels for pre-processing, and 10 channels for classification. In the systems 4 and 5, i.e. without CSP, the number of features is therefore 100. Across the six binary classification tasks, the average accuracy is 78.75 ± 11.82, 82.36 ± 11.05, 80.92 ± 11.13, 70.64 ± 11.15, and 70.90 ± 11.66 with the five feature extraction systems. Post-hoc analyses with a Wilcoxon signed rank test indicated that the solution 2, i.e., to apply CSD on the raw signal, provides the best performance. Without CSP, there was no difference between applying CSD after or before bandpassed signals. Finally, the results confirm the impact of CSP in the increase of the accuracy.

This article has been accepted for publication in a future issue of this journal, but has not been fully edited. Content may change prior to final publication. Citation information: DOI 10.1109/TNSRE.2017.2726779, IEEE Transactions on Neural Systems and Rehabilitation Engineering

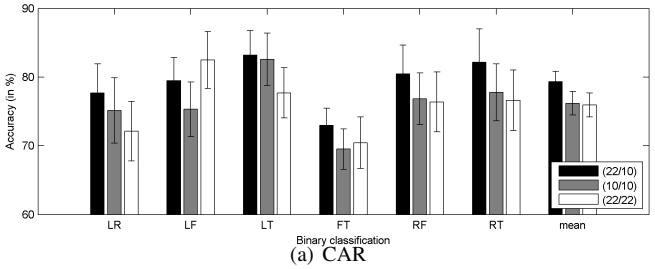

(a) CAR

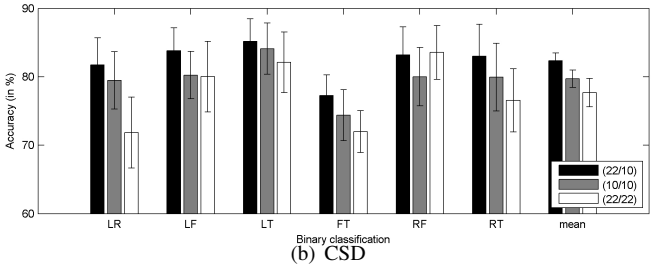

(b) CSD

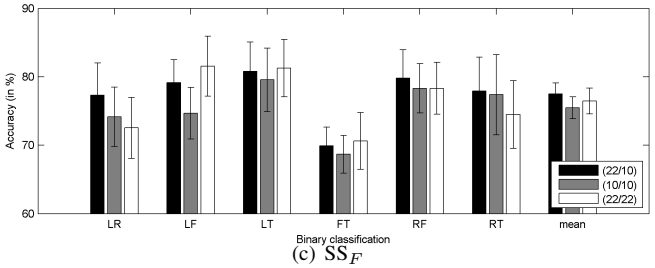

(c) SS_F

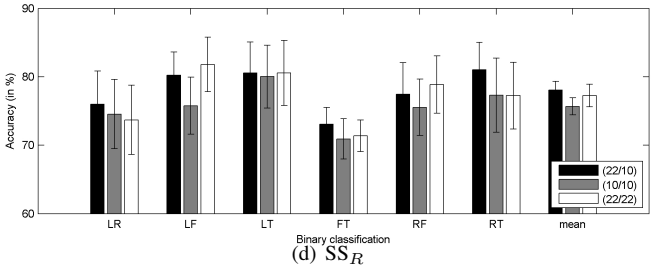

(d) SS_R

Fig. 4. Difference of performance in relation to the number of sensors selected for pre-processing and classification. The couple (Ns0/Ns1) denotes the number of sensors used for pre-processing (Ns0) and for feature extraction (Ns1). The error bars represent the standard error across subjects.

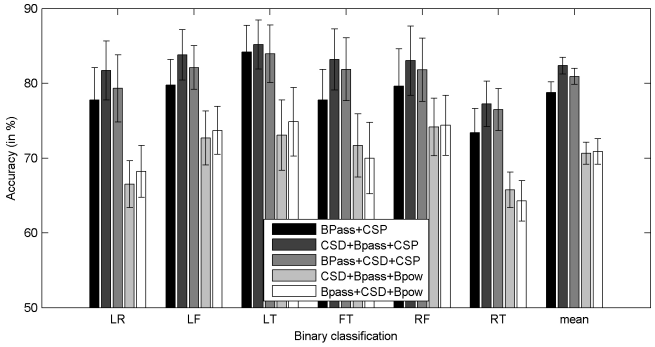

Fig. 5. Difference of performance in relation to the position of CSD in the feature extraction pipeline. The error bars represent the standard error across subjects.

V. Discussion and conclusion

Pre-processing methods are often overlooked and the focus for improving MI based BCI has been mainly on feature extraction techniques that maximize the difference between two classes. Although, with the present study, we found that the feature extraction methods do play a major role in improving classification accuracy, implementing efficient pre-processing techniques can further enhance the performance of a BCI system. Five different pre-processing methods, namely, common reference, common average reference, current source density, finite-difference, and spherical surface Laplacian with realistic head geometry, have been compared in order to address their effect on FBCSP based MI-related BCI performance. More particularly, we have shown that current source density provides improvement of about 3% (in case two-class approach) and 6% (in case four-class approach) compared to the widely used common average referencing. Moreover, the study also estimates the effect of varying the number of EEG channels distinctly during pre-processing stage and feature extraction stage. As we included various distinct algorithms in our signal processing pipeline (i.e. CSD, bandpass filtering, and CSP) which can be positioned in several ways, the impact of all possible combinations, for instance, changing the position of CSD (the winning pre-processing method) and utilising the technique with and without FBCSP on the performance of MI-related BCI has also been studied.

Our analysis yielded several major outcomes. The comparative analysis of all the six binary BCI classification accuracies and four-class classification approach for (22/10) combination showed better performance of CSD method as compared to other methods. Furthermore, the performance differences are statistically significant in five out of six comparisons. A recent study also showed better efficiency of CSD than finite-difference (SS_F) as well as CAR method for counteracting muscular noise in scalp EEG signals [36]. Grand averaged (across all subjects and all binary classifications) analysis of performances showed CAR and CR as better pre-processing methods as compared to SS_F and SS_R. The results related to the impact of the number of channels for pre-processing and feature extraction (classification) indicated three key findings. First, choosing a large number of channels at pre-processing stage (possibly whole scalp coverage) and confining to the motor cortex related channels during feature extraction, yielded better classification accuracies for all the Laplacian methods as compared to other combinations. Second, the efficiency of all the methods reduced significantly with a decrease in the number of channels considered during the pre-processing (e.g. from (22/10) to (10/10)), showing the importance of acquiring the signal with a large number of channels. Third, the number of channels for classification should be reduced after the Laplacian methods as the inclusion of all the channels add redundant information to the classifier (the performance of the (22/10) was better than (22/22)). The study involving variation in the position of CSD method in EEG signal processing pipeline displayed that applying the bandpass filtering before CSD decreased the classification accuracies in all six comparisons and hence supports the utilisation of CSD as the

first step in the pipeline. Finally, CSD with FBCSP enhanced the grand mean accuracy by approximately 17% as compared to CSD without CSP.

There are several limitations to be considered while using surface Laplacian for BCI systems and and can be taken into account in future studies. First, montage density of EEG data is a critical consideration, affecting both the surface potential and surface Laplacian estimates [49]. A dense electrode array EEG montage (64 or more electrodes), providing whole head coverage and with inter-electrode distances less than 2 cm, are generally preferred to a low-density EEG montage (less than 21) with inter-electrode distances greater than 6 cm [36]. Perhaps, this issue can be seen as a possible cause of the reduced effectiveness of the two other Laplacian methods other than CSD (i.e SS_F and SS_R). But for BCI application, affording high-density montage may not be a suitable choice for varied reasons, e.g., high preparation time, subject inconvenience and it adds to the computational complexity of the system. Second, the pursuit of the maximum accuracy in estimation of the surface Laplacian has strengthened the predominant consideration of high spatial sampling of the EEG signal in particular to avoid spatial aliasing and other topographic misrepresentations [50], [51]. However, this principle either rejects the usefulness of low density or it overlooks the evidence that the surface Laplacian transform still renders more useful EEG measures than those obtained from direct surface potentials. Here, we consider that the usefulness of surface Laplacian must be determined with regards to the research objective and in the case of BCI research, their effectiveness can majorly be assessed in terms of the classification accuracy to predict the targeted identity. Third, with surface Laplacian pre-processing, several studies showed suppression of low spatial frequency (i.e., originating from deep and/or distributed generator sources) by the Laplacian effect of spatial high-pass filtering. Although the phenomenon has been studied for EEG coherency, its possible effect on spatial filtering based feature extraction methods (as for FBCSP) still needs to be determined [52].

BCI illiteracy is a significant issue in BCI, and new robust methods have to be proposed to improve the accuracy of command detection. Thanks to CSD, we have shown that it is possible to significantly improve the performance of both binary classification tasks and multi-class classification task accuracies. Because the method depends only on the position of the sensors on the scalp, and not the paradigm itself, it can be easily used and integrated into a signal processing pipeline for motor imagery detection. Finally,the methods described in this study are already available in freely accessible toolboxes (e.g. CSD toolbox, SSLtool, and Fieldtrip), and they are therefore ready to be used within a signal processing framework dedicated to the recognition of motor imagery for BCI [22], [47], [48].

Acknowledgment

D.R. is supported by Ulster University Vice Chancellor's Research scholarship (VCRS). G.P. and H.C. are supported by the Northern Ireland Functional Brain Mapping Facility project (1303/101154803), funded by InvestNI and the University of Ulster. G.P. is also supported by the UKIERI DST Thematic Partnership project "A BCI operated hand exoskeleton based neuro-rehabilitation system" (UKIERI-DST-2013-14/126).

REFERENCES

[1] N. Birbaumer *et al.*, "A spelling device for the paralysed," *Nature*, vol. 398, no. 6725, pp. 297–298, 1999.

[2] J. R. Wolpaw *et al.*, "An eeg-based brain-computer interface for cursor control," *Electroencephalogr. Clin. Neurophysiol.*, vol. 78, no. 3, pp. 252–259, 1991.

[3] G. Pfurtscheller *et al.*, "Brain-computer interface – a new communication device for handicapped persons," *J. Microcomput. Appl*, vol. 16, no. 3, pp. 293–299, 1993.

[4] H. Cecotti, "A self-paced and calibration-less SSVEP-based brain–computer interface speller," *IEEE Trans. Neural Syst. and Rehabil. Eng.*, vol. 18, no. 2, pp. 127–133, 2010.

[5] H. Cecotti and A. Graser, "Convolutional neural networks for p300 detection with application to brain-computer interfaces," *IEEE Trans. Pattern Anal. Mach. Intell.*, vol. 33, no. 3, pp. 433–445, 2011.

[6] B. Blankertz *et al.*, "The BCI competition III: Validating alternative approaches to actual BCI problems," *IEEE Trans. Neural Syst. and Rehabil. Eng.*, vol. 14, no. 2, pp. 153–159, 2006.

[7] D. Rathee *et al.*, "Single-trial effective brain connectivity patterns enhance discriminability of mental imagery tasks," *Journal of Neural Engineering*, 2017.

[8] D. J. McFarland *et al.*, "Electroencephalographic (EEG) control of three-dimensional movement," *J. Neural Eng.*, vol. 7, no. 3, p. 036007, 2010.

[9] B. He *et al.*, "Noninvasive brain-computer interfaces based on sensorimotor rhythms," *Proceedings of the IEEE*, vol. 103, no. 6, pp. 907–925, 2015.

[10] A. Schlögl *et al.*, "Characterization of four-class motor imagery EEG data for the BCI-competition 2005," *J. Neural Eng.*, vol. 2, no. 4, p. L14, 2005.

[11] H. Raza *et al.*, "Adaptive learning with covariate shift-detection for motor imagery-based brain–computer interface," *Soft Computing*, pp. 1–12, 2015.

[12] W. Wu *et al.*, "Probabilistic common spatial patterns for multichannel EEG analysis," *IEEE Trans. Pattern Anal. Mach. Intell.*, vol. 37, no. 3, pp. 639–653, 2015.

[13] F. Qi *et al.*, "RSTFC: A novel algorithm for spatio-temporal filtering and classification of single-trial EEG," *IEEE Trans. Neural Netw. Learn. Syst*, vol. 26, no. 12, pp. 3070–3082, 2015.

[14] H. Raza *et al.*, "EWMA model based shift-detection methods for detecting covariate shifts in non-stationary environments," *Pattern Recognition*, vol. 48, no. 3, pp. 659–669, Aug. 2015.

[15] D. J. McFarland, "The advantages of the surface laplacian in brain–computer interface research," *Int. J. Psychophysiol.*, vol. 97, no. 3, pp. 271–276, 2015.

[16] S. P. van den Broek *et al.*, "Volume conduction effects in EEG and MEG," *Electroencephalogr. Clin. Neurophysiol.*, vol. 106, no. 6, pp. 522–534, 1998.

[17] P. L. Nunez and R. Srinivasan, *Electric fields of the brain: the neurophysics of EEG*. Oxford University Press, USA, 2006.

[18] R. Srinivasan *et al.*, "Spatial sampling and filtering of EEG with spline laplacians to estimate cortical potentials," *Brain Topogr.*, vol. 8, no. 4, pp. 355–366, 1996.

[19] B. Hjorth, "An on-line transformation of EEG scalp potentials into orthogonal source derivations," *Electroencephalogr. Clin. Neurophysiol.*, vol. 39, no. 5, pp. 526–530, 1975.

[20] F. Perrin *et al.*, "Spherical splines for scalp potential and current density mapping," *Electroencephalogr. Clin. Neurophysiol.*, vol. 72, no. 2, pp. 184–187, 1989.

[21] S. Law *et al.*, "High-resolution EEG using spline generated surface laplacians on spherical and ellipsoidal surfaces," *IEEE Trans. Biomed. Eng.*, vol. 40, no. 2, pp. 145–153, 1993.

[22] S. Deng *et al.*, "Improved surface laplacian estimates of cortical potential using realistic models of head geometry," *IEEE Trans. Biomed. Eng.*, vol. 59, no. 11, pp. 2979–2985, 2012.

[23] A. Bashashati *et al.*, "A survey of signal processing algorithms in brain–computer interfaces based on electrical brain signals," *J. Neural Eng.*, vol. 4, no. 2, p. R32, 2007.

[24] Y. Wang and T.-P. Jung, "Improving brain–computer interfaces using independent component analysis," in *Towards Practical Brain-Computer Interfaces*. Springer, 2012, pp. 67–83.

[25] C. Guan *et al.*, "High performance p300 speller for brain-computer interface," in *Biomed. Circuits and Syst., 2004 IEEE Int. Workshop on*. IEEE, 2004, pp. S3–5.

[26] W. Staljanssens *et al.*, "EEG beamforming to extract better features of motor imagery in a two-class real-time BCI," in *Int. Conf. on Basic and Clinical Multimodal Imaging*, vol. 20, no. 10. SAGE, 2013, pp. 108–109.

[27] V. S. Handiru *et al.*, "Cortical source localization for analysing single-trial motor imagery EEG," in *Systems, Man, and Cybernetics (SMC), 2015 IEEE Int. Conf. on*. IEEE, 2015, pp. 3146–3151.

[28] C. Dinh *et al.*, "Real-time MEG source localization using regional clustering," *Brain Topogr.*, vol. 28, no. 6, pp. 771–784, 2015.

[29] B. J. Edelman *et al.*, "EEG source imaging enhances the decoding of complex right-hand motor imagery tasks," *IEEE Trans. Biomed. Eng*, vol. 63, no. 1, pp. 4–14, 2016.

[30] F. Cincotti *et al.*, "High-resolution EEG techniques for brain–computer interface applications," *J. Neurosci. Methods*, vol. 167, no. 1, pp. 31–42, 2008.

[31] C. E. Tenke and J. Kayser, "Generator localization by current source density (CSD): implications of volume conduction and field closure at intracranial and scalp resolutions," *Clin. Neurophysiol.*, vol. 123, no. 12, pp. 2328–2345, 2012.

[32] C. Carvalhaes and J. A. de Barros, "The surface laplacian technique in EEG: theory and methods," *Int. J. Psychophysiol.*, vol. 97, no. 3, pp. 174–188, 2015.

[33] F. Vidal *et al.*, "Linking EEG signals, brain functions and mental operations: Advantages of the laplacian transformation," *Int. J. Psychophysiol.*, vol. 97, no. 3, pp. 221–232, 2015.

[34] G. Shou and L. Ding, "Detection of EEG spatial–spectral–temporal signatures of errors: A comparative study of ICA-based and channel-based methods," *Brain Topogr.*, vol. 28, no. 1, pp. 47–61, 2015.

[35] M. X. Cohen, "Comparison of different spatial transformations applied to EEG data: A case study of error processing," *Int. J. Psychophysiol.*, vol. 97, no. 3, pp. 245–257, 2015.

[36] S. P. Fitzgibbon *et al.*, "Surface laplacian of central scalp electrical signals is insensitive to muscle contamination," *IEEE Trans. Biomed. Eng.*, vol. 60, no. 1, pp. 4–9, 2013.

[37] B. Binias *et al.*, "Elimination of bioelectrical source overlapping effects from the EEG measurements," in *2016 17th Int. Carpathian Control Conf. (ICCC)*. IEEE, 2016, pp. 70–75.

[38] T. F. Oostendorp and A. van Oosterom, "The surface laplacian of the potential: theory and application," *IEEE Trans. Biomed. Eng.*, vol. 43, no. 4, pp. 394–405, 1996.

[39] F. Perrin *et al.*, "Scalp current density mapping: value and estimation from potential data," *IEEE Trans. Biomed. Eng.*, no. 4, pp. 283–288, 1987.

[40] C. Tenke *et al.*, "Response-and stimulus-related ERP asymmetries in a tonal oddball task: a laplacian analysis," *Brain Topogr.*, vol. 10, no. 3, pp. 201–210, 1998.

[41] D. J. McFarland *et al.*, "Spatial filter selection for eeg-based communication," *Electroencephalogr. Clin. Neurophysiol.*, vol. 103, no. 3, pp. 386–394, 1997.

[42] O. Bertrand *et al.*, "A theoretical justification of the average reference in topographic evoked potential studies," *Electroencephalogr. Clin. Neurophysiol./Evoked Potentials Section*, vol. 62, no. 6, pp. 462–464, 1985.

[43] G. Huiskamp, "Difference formulas for the surface laplacian on a triangulated surface," *J. Comput. Phys.*, vol. 95, no. 2, pp. 477–496, 1991.

[44] N. Max, "Weights for computing vertex normals from facet normals," *J. of Graphics Tools*, vol. 4, no. 2, pp. 1–6, 1999.

[45] M. Tangermann *et al.*, "Review of the BCI competition IV," *Front. Neurosci.*, vol. 6, p. 55, 2012.

[46] K. K. Ang *et al.*, "Filter bank common spatial pattern algorithm on BCI competition IV datasets 2a and 2b," *Front. Neurosci.*, vol. 6, p. 39, 2012.

[47] R. Oostenveld *et al.*, "Fieldtrip: open source software for advanced analysis of MEG, EEG, and invasive electrophysiological data," *Comput. Intell. Neurosci.*, vol. 2011, 2010.

[48] J. Kayser, "Current source density (CSD) interpolation using spherical splines–CSD toolbox (version 1.1)," *New York State Psychiatric Institute: Division of Cognitive Neuroscience*, 2009.

[49] J. Kayser and C. E. Tenke, "Issues and considerations for using the scalp surface laplacian in EEG/ERP research: A tutorial review," *Int. J. Psychophysiol.*, vol. 97, no. 3, pp. 189–209, 2015.

[50] M. Junghöfer *et al.*, "Mapping EEG potentials on the surface of the brain: a strategy for uncovering cortical sources," *Brain Topogr.*, vol. 9, no. 3, pp. 203–217, 1997.

[51] P. L. Nunez and A. F. Westdorp, "The surface laplacian, high resolution EEG and controversies," *Brain Topogr.*, vol. 6, no. 3, pp. 221–226, 1994.

[52] P. L. Nunez *et al.*, "EEG coherency-I: statistics, reference electrode, volume conduction, laplacians, cortical imaging, and interpretation at multiple scales," *Electroencephalogr. Clin. Neurophysiol.*, vol. 103, no. 5, pp. 499–515, 1997.